

Journal of Geophysical Research: Atmospheres**RESEARCH ARTICLE**

10.1002/2013JD020997

Key Points:

- Realistic annual cycle of dust in CESM compared to observations
- Strong summer correlation between dust and low clouds downstream of North Africa
- Dust burden at 700 hPa enhances low cloud cover by increasing inversion strength

Correspondence to:M. J. DeFlorio,
mdeflori@ucsd.edu**Citation:**

DeFlorio, M. J., S. J. Ghan, B. Singh, A. J. Miller, D. R. Cayan, L. M. Russell, and R. C. J. Somerville (2014), Semidirect dynamical and radiative effect of North African dust transport on lower tropospheric clouds over the subtropical North Atlantic in CESM 1.0, *J. Geophys. Res. Atmos.*, 119, 8284–8303, doi:10.1002/2013JD020997.

Received 3 OCT 2013

Accepted 31 MAY 2014

Accepted article online 4 JUN 2014

Published online 9 JUL 2014

Semidirect dynamical and radiative effect of North African dust transport on lower tropospheric clouds over the subtropical North Atlantic in CESM 1.0

Michael J. DeFlorio¹, Steven J. Ghan², Balwinder Singh², Arthur J. Miller¹, Daniel R. Cayan^{1,3}, Lynn M. Russell¹, and Richard C. J. Somerville¹

¹Climate, Atmospheric Science, and Physical Oceanography, Scripps Institution of Oceanography, University of California, San Diego, California, USA, ²ASGC Division, Pacific Northwest National Laboratory, Richland, Washington, USA, ³Water Resources Discipline, U.S. Geological Survey, La Jolla, California, USA

Abstract This study uses a century length preindustrial climate simulation by the Community Earth System Model (CESM 1.0) to explore statistical relationships between dust, clouds, and atmospheric circulation and to suggest a semidirect dynamical mechanism linking subtropical North Atlantic lower tropospheric cloud cover with North African dust transport. The length of the run allows us to account for interannual variability of North African dust emissions and transport in the model. CESM's monthly climatology of both aerosol optical depth and surface dust concentration at Cape Verde and Barbados, respectively, agree well with available observations, as does the aerosol size distribution at Cape Verde. In addition, CESM shows strong seasonal cycles of dust burden and lower tropospheric cloud fraction, with maximum values occurring during boreal summer, when a strong correlation between these two variables exists over the subtropical North Atlantic. Calculations of Estimated Inversion Strength (EIS) and composites of EIS on high and low downstream North African dust months during boreal summer reveal that dust is likely increasing inversion strength over this region due to both solar absorption and reflection. We find no evidence for a microphysical link between dust and lower tropospheric clouds in this region. These results yield new insight over an extensive period of time into the complex relationship between North African dust and North Atlantic lower tropospheric clouds, which has previously been hindered by spatiotemporal constraints of observations. Our findings lay a framework for future analyses using different climate models and submonthly data over regions with different underlying dynamics.

1. Introduction

The role of aerosols in the climate system is complex, and their forcing on the climate system remains a large uncertainty in model projections of climate change [Stevens and Feingold, 2009]. Aerosols originate from a variety of natural and anthropogenic sources and induce both direct (via scattering, reflection, and absorption) and indirect (via cloud seeding) effects on Earth's radiative budget [Twomey, 1974; Albrecht, 1989; Leaitch *et al.*, 1992; Kiehl and Briegleb, 1993; Jones *et al.*, 1994; Lohmann and Feichter, 2005; Carslaw *et al.*, 2010].

Mineral dust in particular interacts with local and remote climate in a variety of ways. It is an effective absorber and scatterer of incoming shortwave radiation and an effective absorber and emitter of outgoing terrestrial longwave radiation [Tegen *et al.*, 1996; Penner *et al.*, 2001; Sokolik *et al.*, 2001; Tegen, 2003] and has been linked to modification of cloud properties and precipitation [e.g., Kaufman *et al.*, 2005]. Dust has been shown to suppress precipitation by acting as cloud condensation nuclei (CCN) that decrease droplet size [Rosenfeld *et al.*, 2001] and to alter radiative and meteorological characteristics of upper tropospheric clouds by serving as ice condensation nuclei [DeMott *et al.*, 2003; Sassen *et al.*, 2003; Smoydzin *et al.*, 2012]. The impact of dust on cold phase clouds and subsequent precipitation has received considerable attention recently, as several studies have examined the remote influence of transported Asian dust on heavy orographically enhanced precipitation over the Sierra mountain range [Rosenfeld *et al.*, 2008; Ault *et al.*, 2011].

The largest global source of dust is the North African Sahel-Sahara desert region, which emits approximately 800 Tg of dust each year [Huneeus *et al.*, 2011]. Consequently, the impact of North African dust on global climate has received considerable attention over the past several decades and has spawned a number of biogeochemical, meteorological, and climatic studies that focus on the effect of

mineral dust on clouds, circulation, and radiation both locally and in remote regions downwind of dust sources [Prospero and Nees, 1986; Martin, 1990; Okin *et al.*, 2004; Chiapello *et al.*, 2005; Evan and Mukhopadhyay, 2010; Mahowald *et al.*, 2010].

This transport of mineral dust in Earth's atmosphere downwind of arid high source regions has been observed for centuries. Nineteenth and early-to-middle twentieth century observations were made by ships [Darwin, 1897; Prospero and Bonatti, 1968] or by land stations that measured advected dust [Prospero *et al.*, 1970]. Many subsequent studies of observed mineral dust were greatly aided by the onset of the satellite era and the development of remote sensing techniques for mineral aerosols [Ackerman and Chung, 1992; Moulin *et al.*, 1997; Evan *et al.*, 2006]. These improvements allowed for the detection of dust over the ocean at improved spatial resolutions, spanning longer continuous periods of time. Specific to the North African region, Evan and Mukhopadhyay [2010] implemented a simple statistical model to extend satellite-retrieved dust measurements over the northern tropical Atlantic from 1955 to 2008.

Despite these improvements, it remains challenging to obtain a coherent spatiotemporal record of dust, circulation, and clouds over North Africa and the tropical-subtropical North Atlantic that is extensive enough to calculate robust statistics that are of sufficient length to address climate-related questions. To provide such a record, this study uses oceanic and atmospheric output from a state-of-the-art century length global coupled climate model simulation with an interactive aerosol treatment to address several important questions: (a) What are the characteristics of seasonal variability in dust emissions, dust transport, and other relevant meteorological variables over North Africa and the North Atlantic basin? (b) Is there a multiyear mode of variability in the emissions and transport of dust over North Africa, and is the interannual variability stronger during particular seasons? (c) How are North African dust emissions and transport related to lower tropospheric stratiform clouds over the tropical and subtropical North Atlantic, downstream of high dust source regions? (d) Does dust residing in the lower troposphere in boreal summer promote boundary layer stratiform cloud growth by strengthening the inversion in the lower troposphere downstream of North Africa?

These questions are important because the response of radiative forcing of optically thick stratiform clouds in the lower troposphere to climate change is still one of the largest sources of uncertainty in climate models [Yokohata *et al.*, 2010; Klocke *et al.*, 2011]. In addition, enhanced lower tropospheric cloud growth due to increased dust transport could further decrease the likelihood of hurricane formation in the Atlantic due to reduced sea surface temperature [Evan *et al.*, 2009], which has the potential to strongly impact the economy of Caribbean island nations, Mexico, and the eastern United States.

This is the first study to use a century length coupled model simulation with an interactive modal aerosol treatment to explore statistical relationships between North African dust, clouds, and circulation. The Community Earth System Model (CESM 1.0) [Hurrell *et al.*, 2013] is chosen for this study because of its inclusion of the aerosol indirect effect and its ability to capture observed spatiotemporal variability of aerosol mass and number concentrations, size distributions, and aerosol optical properties [Liu *et al.*, 2012]. Our results suggest a dynamical and radiative, rather than microphysical, mechanism linking subtropical North Atlantic lower tropospheric cloud cover with dust transported from North Africa. This semidirect mechanism is similar to the one identified by Koch and Del Genio [2010] for black carbon aerosols.

2. Data Used

2.1. CESM 1.0 150 Year Simulation

We ran a 150 year preindustrial global simulation using CESM 1.0.3 (<http://www2.cesm.ucar.edu>) with interactive dust emission and transport, which allows dust as well as other components of the aerosol to affect radiative budgets and cloud properties at each time step [Hurrell *et al.*, 2013]. The simulation was run at a horizontal resolution of 2.5° (longitude (lon)) $\times 1.9^\circ$ (latitude (lat)). The component set for this simulation is "1.9x2.5_gx1v6_B_1850_CAM5_CN," and the code base is CESM 1.0.3. Monthly simulation output was saved for several species of aerosols, including mineral dust (e.g., surface emissions, optical depth, atmospheric burdens, absorption, and vertical concentrations) and associated variables relevant to understanding aerosol and cloud processes. This CESM simulation features a realistic seasonal cycle of dust and African easterly jet formation and improved parameterizations of boundary layer clouds and cloud microphysics [Bretherton and Park, 2009; Park and Bretherton, 2009; Gent *et al.*, 2011; Neale *et al.*, 2013; Hurrell *et al.*, 2013].

Table 1. Trimodal Aerosol Treatment in CESM 1.0^a

Aitken	Accumulation	Coarse
Sulfate	Sulfate	Soil dust
Secondary OM	Secondary OM	Sea salt
Sea salt	Primary OM Black carbon Soil dust Sea salt	Sulfate

^aTrimodal treatment of aerosols in century length interactive CESM 1.0 runs similar to the one used in this study.

A century length simulation is necessary due to interannual variability of boreal summer dust emissions and transport over the North African and eastern subtropical North Atlantic associated with the El Niño–Southern Oscillation in CESM (not shown).

2.2. CAM5 Trimodal Treatment of Aerosols in Long CESM Runs

For extensive climate runs (decades to millennia), Community Atmosphere Model (CAM5) treats

aerosols using a trimodal aerosol module that includes an Aitken (small), accumulation (medium), and coarse (large) mode representation of aerosol species. Table 1 lists the species in each mode, whose properties are predicted forward in time over the course of the simulation (see Liu *et al.* [2012] for more details). Mineral dust is emitted in both the coarse and accumulation modes using the Zender *et al.* [2003] Dust Entrainment and Deposition Model, as described by Liu *et al.* [2012]. The cutoff size range for dust emissions is 0.1–1.0 μm for the accumulation mode, and 1.0–10 μm for coarse. Dust is assumed to be internally mixed with the other components in each mode, with the bulk hygroscopicity and refractive index of each mode calculated assuming volume mixing of the hygroscopicity and refractive index values of each component (including water in the case of refractive index) in the mode. Water uptake is calculated using κ -Kohler theory [Petters and Kreidenweis, 2007]. Volume mixing enhances absorption by dust when coated with sulfate, organic, and water. The hygroscopicity (κ) for mineral dust is specified as 0.068, while the dust refractive indices are from Optical Properties of Aerosols and Clouds (OPAC) [Hess *et al.*, 1998]. The imaginary part of the refractive index for the OPAC dust is known to be greater than that retrieved for Saharan dust [Sinyuk *et al.*, 2003], so excessive absorption by dust in the simulation should be kept in mind. Dust optical properties (extinction efficiency, absorption efficiency, and asymmetry factor) are parameterized from Mie calculations [Ghan and Zaveri, 2007]. Dust is transported by the resolved winds, vertical diffusion, and cumulus mass flux in CAM5 and removed by dry deposition, nucleation scavenging, and impact scavenging as described by Liu *et al.* [2012].

2.3. NASA AERONET Observational Data Set

We evaluate aerosol optical depth and volume size distribution in CAM5 using approximately 20 years of NASA AERONET (Aerosol Robotic Network) Version 2 Direct Sun Algorithm and Inversions data (Level 2.0) collected at Cape Verde (16°N, –22°W) (http://aeronet.gsfc.nasa.gov/new_web/index.html). Station data at this site are available from January 1996 to April 2013 and were quality controlled to distinguish between aerosol and cloud [Smirnov *et al.*, 2001]. Prefield and postfield calibrations were applied to the aerosol optical depth (AOD) data, which were also automatically cloud cleared and manually inspected for quality control. The data set at Cape Verde is limited by an instrument malfunction, which caused missing data for several months in the 17 year record. We also evaluate AOD at Ragged Point near Barbados (13°N, –60°W), where data are available from August 2007 to April 2014. Retrieval development and implementation techniques for AERONET inversion products were introduced in Dubovik and King [2000].

2.4. Barbados Dust Observational Data Set

We evaluate surface dust concentration in CAM5 by using 44 years of monthly mean data recorded at Barbados from 1965 to 2008 [Prospero and Lamb, 2003]. Recorded concentrations are based on the ash weight of the filter after extracting solubles. The monthly means are comprised of samples where the run time was greater than 10%; samples whose run times were under 10% were not included because of limited data and unreliable surface wind measurements (J. M. P. Prospero, personal communication, 2014).

2.5. ISCCP Cloud Data

For evaluation of lower tropospheric cloud fraction, we use the International Satellite Cloud Climatology Project (ISCCP) D1 series global data set (<http://isccp.giss.nasa.gov/products/dataview.html>), which spans from January 1984 to December 2009 and has a horizontal resolution of 2.5° (lon) \times 2.5° (lat) [Rossow and Schiffer, 1991]. The data set has been corrected for artifacts with normalization and meteorological indices, and the cloud fraction is averaged to monthly values. Although the CALIPSO data set has superior vertical

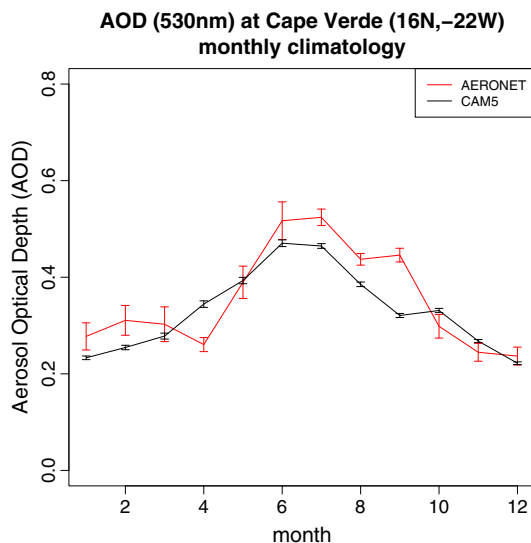


Figure 1. Mean monthly climatology of 530 nm aerosol optical depth (AOD) near Cape Verde (16°N , -22°W) from AERONET (red) and CAM5 (black). The AERONET data are available from 1996 to the present, and the CAM5 simulation is 150 years. Vertical bars represent ± 1 interannual standard error for each month.

determine whether or not its representation of aerosol optical depth (AOD), volume size distribution, and surface dust concentration are in reasonable agreement with limited available observations. For AOD and volume size distribution, we use AERONET observations near Cape Verde; for surface dust concentration, we evaluate CAM5 using the observations from Barbados. This approach gives a sense of the realism of CAM5 dust both near and downstream of the high source region over North Africa.

Most of the AOD near Cape Verde is produced by dust, so AOD is a good indicator of the dust column burden. Figure 1 shows monthly climatologies of 530 nm AOD near Cape Verde (16°N , -22°W) for AERONET (red) and CAM5 (black). Recall that the AERONET data set spans 17 years, while the CAM5 simulation is 150 years long.

resolution, it is only available from 2006 to 2012, which is a major drawback given the length of our CESM simulation.

2.6. Dust Variables Used in This Study

In this study, we will focus on analyzing three dust variables: (A) total atmospheric dust burden (g/m^2), which vertically integrates all dust modes to obtain a column dust mass at each grid cell; (B) accumulation mode dust concentration (kg dust/kg air); and (C) coarse mode dust concentration (kg dust/kg air). (B) and (C) are saved at 30 vertical levels in the atmosphere and allow us to examine the vertical structure of dust over our regions of interest. We calculate seasonal averages of all variables used in this study to discern the strong seasonal cycle of dust observed in the North African region [Prospero and Nees, 1986].

3. Evaluation of CAM5 Aerosol Optical Depth, Volume Size Distribution, and Surface Dust Concentration

Before analyzing CAM5 output, it is important to obtain AERONET AOD at 530 nm by calculating the Angstrom exponent using measurements at 440 nm and 675 nm, since AERONET does not retrieve AOD at 530 nm at Cape Verde. The annual cycle of AOD is similar for all three data sets, though boreal autumn values are approximately 30% higher in AERONET. The error bars are larger for AERONET due in part to the shorter record length relative to CAM5, and the error bars generally increase during the spring and summer. The width of the error bars is larger in summer relative to late fall and winter, which suggests that interannual variability of AOD is larger during summer.

Aerosol particle size affects both atmospheric residence time and physical and chemical properties of aerosols in the atmosphere [Seinfeld and Pandis, 2012]. Therefore, it is important to evaluate CESM aerosol size distribution using available observations. Figure 2 shows the time-averaged column-integrated volume size distribution of aerosols near Cape Verde from

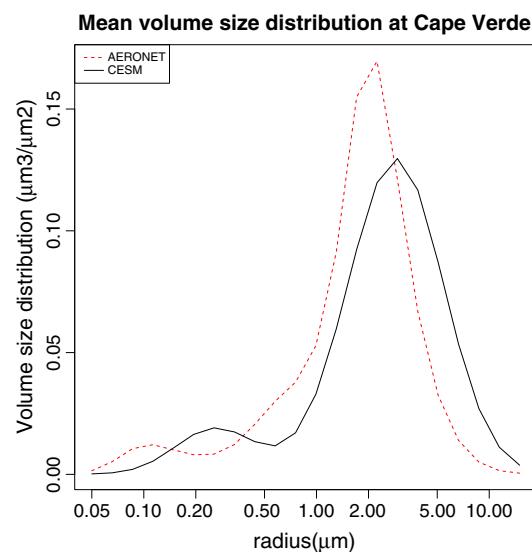


Figure 2. Column-integrated volume size distribution (m^3/m^2) of aerosols at Cape Verde from AERONET (red) and CESM (black).

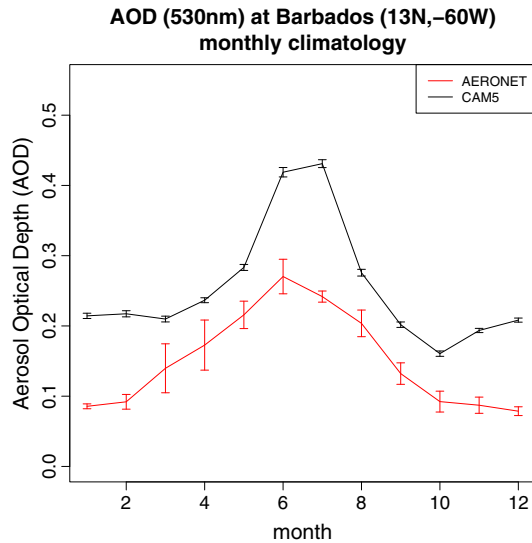


Figure 3. Mean monthly climatology of 530 nm aerosol optical depth (AOD) near Barbados (13°N , -60°W) from AERONET (red) and CAM5 (black). The AERONET data are available from 2007 to the present, and the CAM5 simulation is 150 years. Vertical bars represent ± 1 standard error for each month.

this case, the observations only span 44 years, while the Cape Verde AOD comparison, CAM5's monthly climatology of surface concentration is realistic. The peak in observed surface dust concentration precedes that of the model by approximately 1 month and has larger error bars in all months. The error bars for both observations and CAM5 are largest during boreal summer, when the mean surface dust concentration is highest.

Overall, the model's representation of the seasonal cycle of AOD both near the continental source regions and downstream of the continent near Barbados is quite realistic, with some discrepancies in magnitude. There are several possible explanations for differences between the two distributions. Perhaps the most likely cause is attributable to unreliable emissions in CAM5. In particular, the sources of dust described in Zender *et al.* [2003] do not include sources in the Sahel, a region where local emission contributes substantially to high daily dust concentration at the end of spring and early summer [Marticorena *et al.*, 2010]. In addition, our model does not resolve cold pool downdrafts over the North African region that produce haboobs, which could account for a significant amount of dust emission during the spring to summer transition period [Marticorena *et al.*, 2010; Ashpole and Washington, 2013]. Dust emission is also a complex function of other variables including soil moisture and particle size distribution [Kok, 2011]. Other possible explanations include relatively low dry and wet deposition rates of dust in CAM5 over the North Atlantic, or differences between the observed and modeled horizontal wind field over the open ocean.

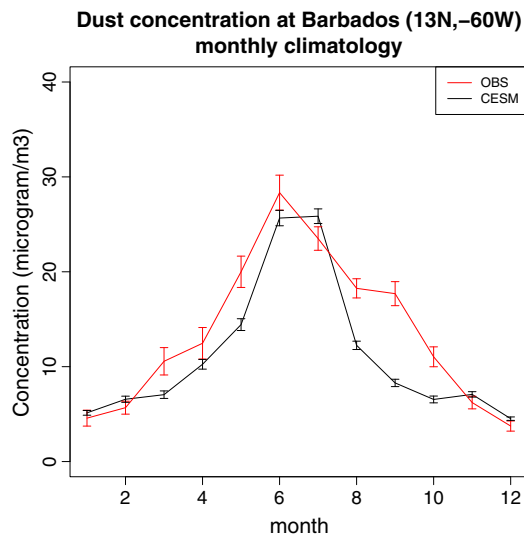


Figure 4. Mean monthly climatology of surface dust concentration ($\mu\text{g}/\text{m}^3$) near Barbados (13°N , -60°W) from AERONET (red) and CAM5 (black). Data at Barbados are available from 1965 to 2008, while the CAM5 simulation is 150 years. Vertical bars represent ± 1 standard error for each month.

AERONET (red) and CESM (black). Both distributions were calculated using 22 bins of logarithmically spaced radii from $0.5 \mu\text{m}$ to $15 \mu\text{m}$ and assuming a lognormal distribution of number mode radius. For CESM data, average volume mixing ratios were calculated for each mode using the aerosol species listed in Table 1. CESM's distribution is biased toward slightly coarser radii, and its standard deviation in the coarse mode is larger. The magnitudes of the distributions are comparable.

It is also useful to evaluate dust in the atmosphere downstream of the high source regions over North Africa. Similar to Figure 1, Figure 3 shows monthly climatologies of 530 nm AOD near Barbados (13°N , -60°W) for AERONET (red) and CAM5 (black). The timing of the seasonal cycle of AOD is similar, with peak values occurring in June and July, but CAM5 overestimates the magnitude of AOD by a factor of 2 across all seasons.

Figure 4 shows monthly climatologies of surface dust concentration ($\mu\text{g}/\text{m}^3$) near Barbados (13°N , -60°W) for observations (red) and CAM5 (black). In the CAM5 simulation is 150 years long. Similar to the Cape Verde AOD comparison, CAM5's monthly climatology of surface concentration is realistic. The peak in observed surface dust concentration precedes that of the model by approximately 1 month and has larger error bars in all months. The error bars for both observations and CAM5 are largest during boreal summer, when the mean surface dust concentration is highest. Overall, the model's representation of the seasonal cycle of AOD both near the continental source regions and downstream of the continent near Barbados is quite realistic, with some discrepancies in magnitude. There are several possible explanations for differences between the two distributions. Perhaps the most likely cause is attributable to unreliable emissions in CAM5. In particular, the sources of dust described in Zender *et al.* [2003] do not include sources in the Sahel, a region where local emission contributes substantially to high daily dust concentration at the end of spring and early summer [Marticorena *et al.*, 2010]. In addition, our model does not resolve cold pool downdrafts over the North African region that produce haboobs, which could account for a significant amount of dust emission during the spring to summer transition period [Marticorena *et al.*, 2010; Ashpole and Washington, 2013]. Dust emission is also a complex function of other variables including soil moisture and particle size distribution [Kok, 2011]. Other possible explanations include relatively low dry and wet deposition rates of dust in CAM5 over the North Atlantic, or differences between the observed and modeled horizontal wind field over the open ocean.

Figure 5 shows histograms of monthly averaged surface dust concentration near Barbados from

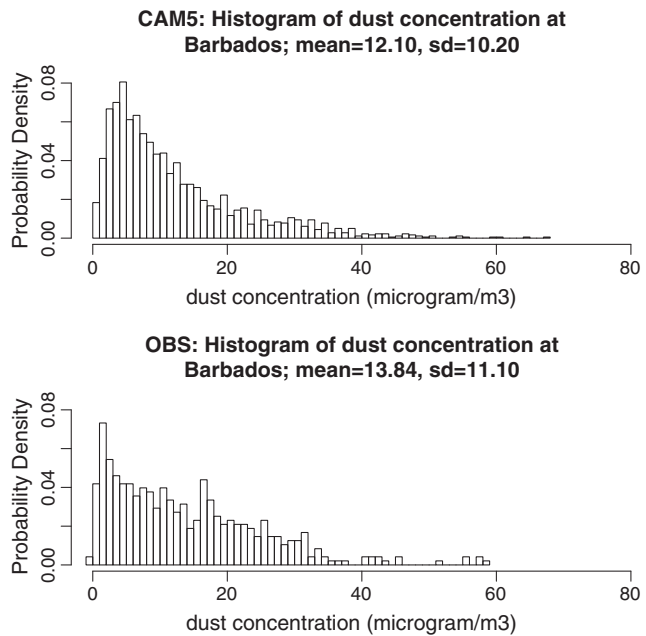


Figure 5. Histograms of dust concentration near Barbados (13°N , -60°W) from (top) CAM5 and from (bottom) observations.

simulation account for 61% of global dust burden in boreal winter, and 68% in boreal summer (not shown). Despite uncertainties and constraints of observations, these percentages are qualitatively similar to observational estimates [Engelstaedter *et al.*, 2006]. We note that our model simulation ignores

CAM5 (top) and observations (bottom). The means and variances of the CAM5 and observed surface dust concentration distributions are very similar, much like the AOD comparison at Cape Verde. Both distributions are positively skewed, though extreme values are larger in CAM5 than in observations. In summary, Figures 1–5 show that the seasonal climatologies and distribution shapes of AOD and surface dust concentration in CAM5 are generally realistic when compared to limited available observations, as is the volume size distribution of aerosols near Cape Verde.

4. Mean Seasonal Climatologies and Vertical Structure of Dust

4.1. Dust Burden

One hundred fifty year averages of dust burden over North Africa in our

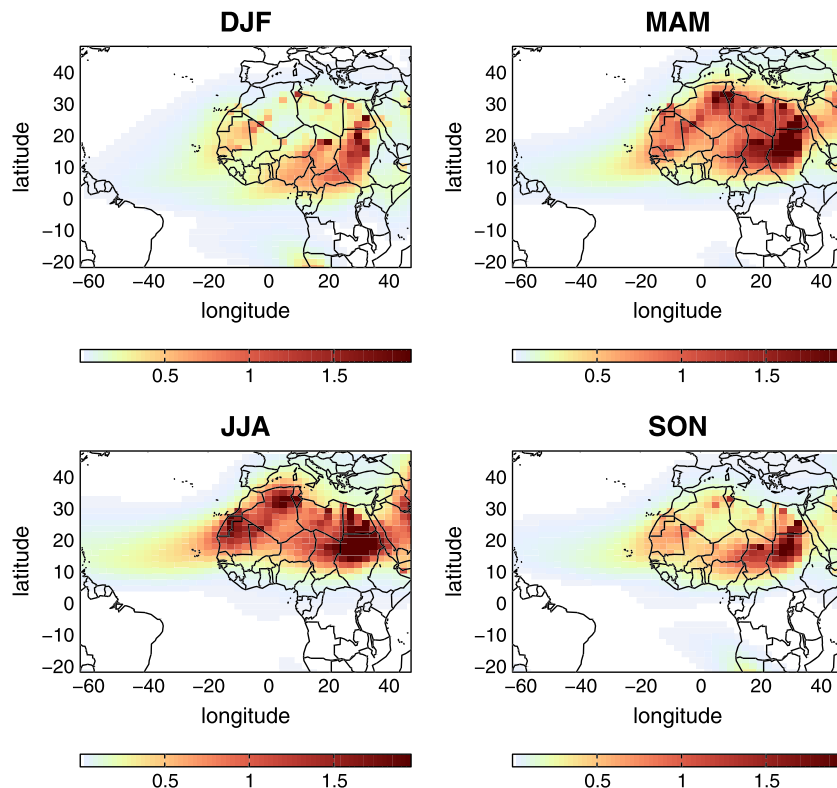


Figure 6. One hundred fifty year seasonal averages of CAM5 total dust burden (g/m^2) for December-January-February (DJF), March-April-May (MAM), June-July-August (JJA), and September-October-November (SON).

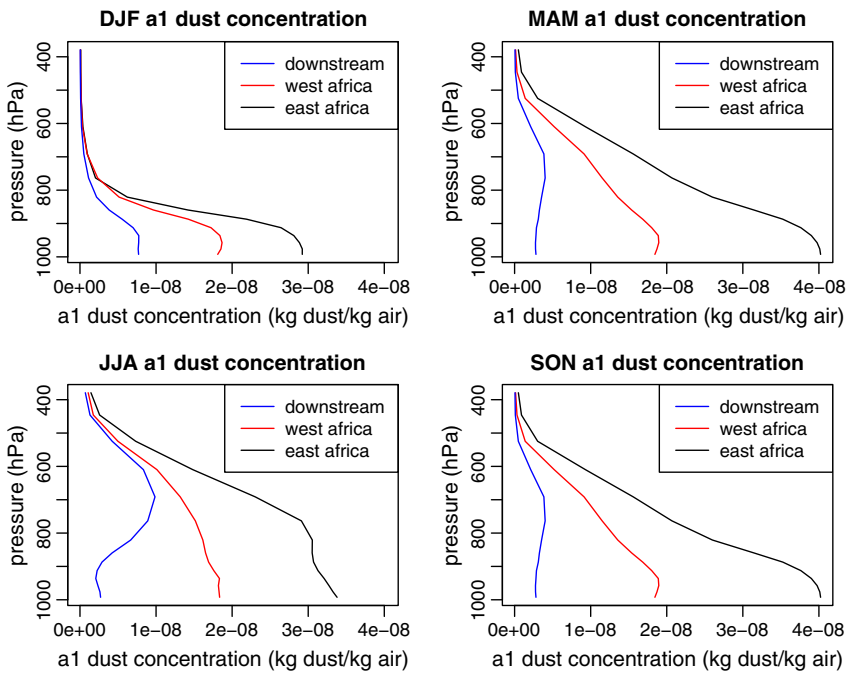


Figure 7. Vertical profiles of 150 year seasonal averages of CAM5 accumulation mode (a1) dust concentration.

anthropogenic sources of dust, which have been estimated to represent 8% of North African dust and 25% of global dust burden [Ginoux *et al.*, 2012]. Additionally, there is a strong seasonal cycle of dust burden and emissions in CESM.

Figure 6 shows 150 year seasonal averages of total dust burden (g/m^2) over North Africa and the tropical-subtropical North Atlantic. Increased atmospheric dust loading during boreal spring and summer and subsequent downstream transport over the open ocean in CESM are consistent with observations from

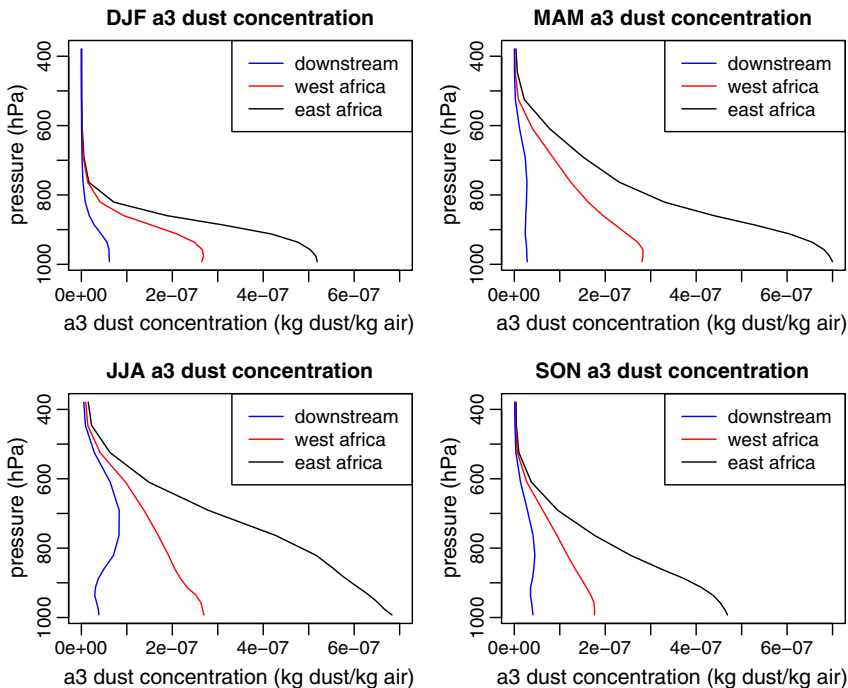


Figure 8. As in Figure 7 but for coarse mode (a3) dust concentration.

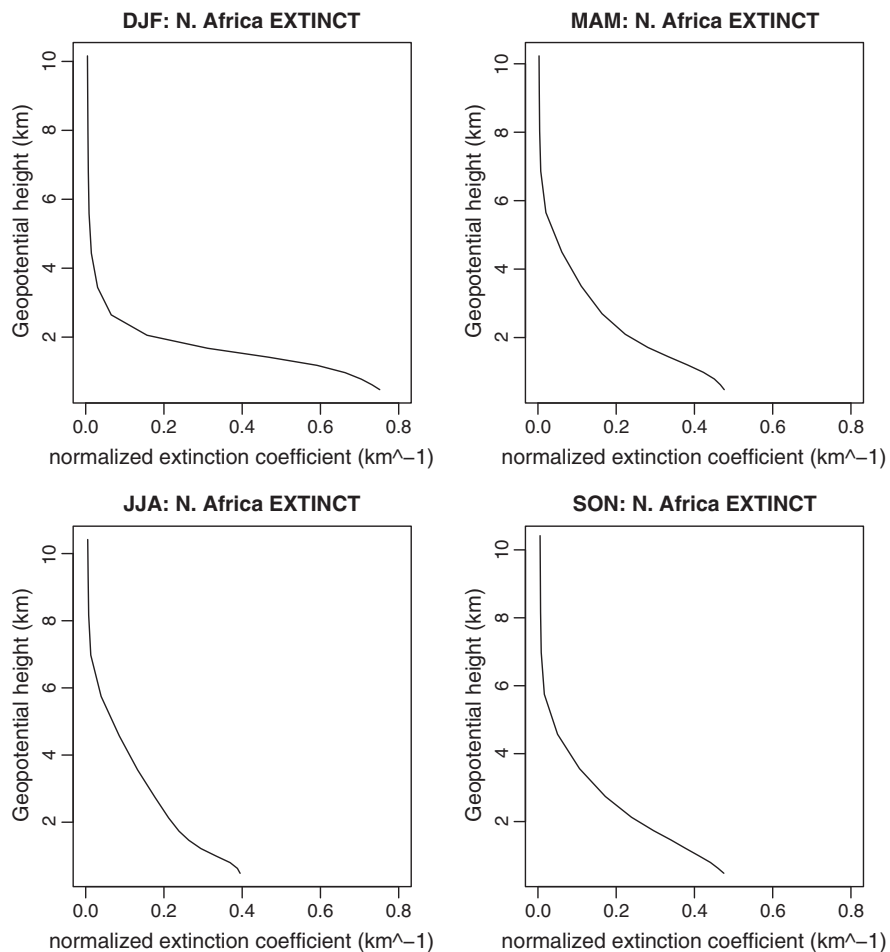


Figure 9. Vertical profiles of 150 year seasonal averages of CAM5 normalized aerosol extinction coefficient (km^{-1}) over North Africa.

previous satellite and in situ based studies (*Engelstaedter et al. [2006]* and *Prospero and Lamb [2003]*, respectively, e.g.), though comparisons between limited spatiotemporal observational data and a century coupled climate model run must be made with caution. Notably, there are three major Saharan dust source regions in the model that are most pronounced during boreal summer: (A) West Africa, near southern Morocco (-20°W to 0°W , 15°N to 30°N), (B) North Africa, near northern Algeria (0°W to 10°W , $\sim 30^{\circ}\text{N}$), and (C) East Africa, near northern Sudan and southern Egypt (20°W to 40°W , 10°N to 25°N). The dust burdens in regions A and C are generally an order of magnitude greater in boreal summer; the burden in region B is near zero during boreal winter, but of comparable magnitude to regions A and C during boreal summer.

4.2. Vertical Structure of Dust Over North Africa and Subtropical North Atlantic

To better understand the zonal and vertical structure of dust transport, Figures 7 and 8 show vertical profiles of 150 year seasonal averages of accumulation mode (a1) and coarse mode (a3) dust concentration, respectively, over the subtropical Atlantic downstream North African region (-35°W to -20°W , 15°N to 25°N ; blue), West Africa (-15°W to -5°W , 15°N to 25°N ; red), and East Africa (20°W to 40°W , 15°N to 25°N ; black). Dust concentrations are highest over the East African surface across all seasons compared to the other two locations. This indicates that dust transport over the open ocean during these seasons is primarily occurring in the lower troposphere, near 700 hPa.

Assessing the realism of Figures 7 and 8 is important, but observational records of the vertical structure of aerosols are very limited. *Koffi et al. [2012]* evaluated Cloud-Aerosol Lidar with Orthogonal Polarization aerosol extinction coefficient profiles at over North Africa and the subtropical North Atlantic from 2007 to 2009 using 12

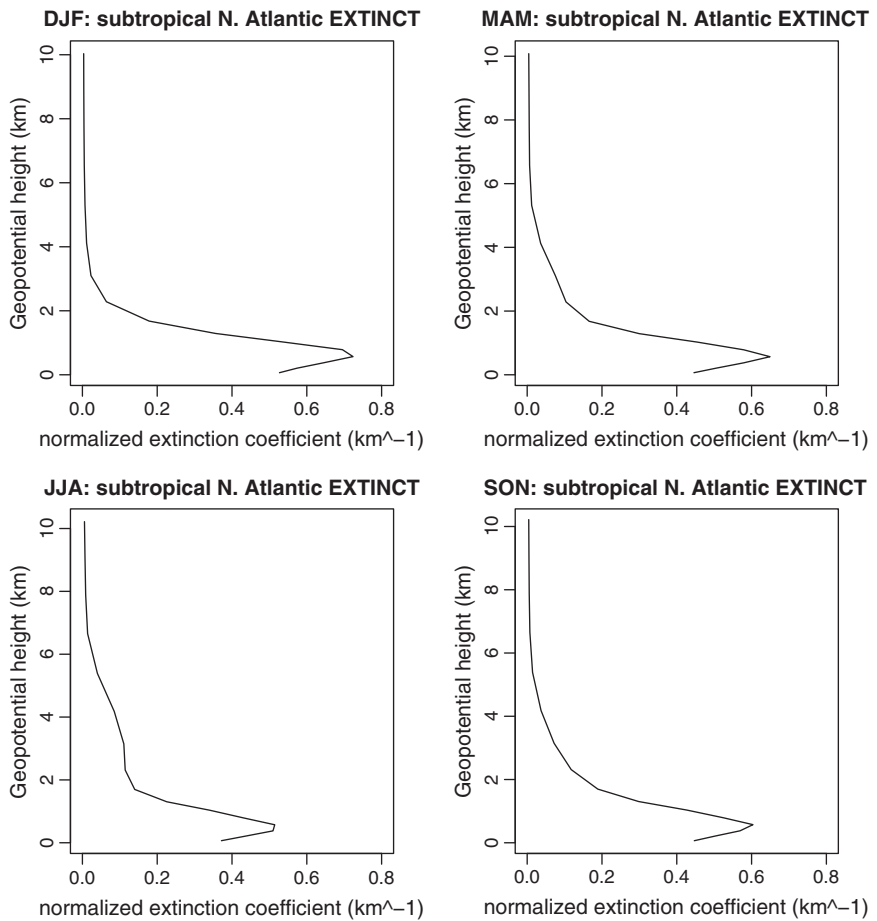


Figure 10. Vertical profiles of 150 year seasonal averages of CAM5 normalized aerosol extinction coefficient (km^{-1}) over the subtropical North Atlantic.

AEROCOM 2000 simulations. Figures 9 and 10 show CESM aerosol extinction coefficient profiles over the North African and subtropical North Atlantic regions defined in Koffi *et al.* [2012]. The values were normalized according to the method described in Koffi *et al.* [2012] such that the total AOD is normalized over the first 10 km of the atmosphere. The vertical structure of CESM aerosol extinction is generally realistic in these regions, especially during boreal summer over the subtropical North Atlantic. Observations used by Koffi *et al.* [2012] show advection of Saharan dust to the Atlantic between 2 and 5 km, which is confirmed by Figures 7–9.

Table 2. Mean Aerosol Extinction Height (km)^a

	CAM5	CALIPSO (Koffi <i>et al.</i> [2012])
NAF DJF	1.10 ± 0.002	1.23
NAF MAM	1.36 ± 0.001	2.10
NAF JJA	1.58 ± 0.001	2.44
NAF SON	1.41 ± 0.003	1.85
CAT DJF	0.75 ± 0.002	1.10
CAT MAM	0.85 ± 0.002	1.33
CAT JJA	1.04 ± 0.003	1.96
CAT SON	0.88 ± 0.002	1.31

^aComparison of mean aerosol extinction height (km) for CAM5 and the CALIPSO data used in Koffi *et al.* [2012] for the North Africa (NAF) and subtropical North Atlantic (CAT) regions. Indicated for CAM5 are ± 1 standard errors.

Table 2 shows a comparison of mean extinction height Z_α for CAM5 and the CALIPSO data used in Koffi *et al.* [2012] over the North African and subtropical North Atlantic regions. Mean extinction height is defined as

$$Z_\alpha = \frac{\sum_{i=1}^n b_{\text{ext},i} \times Z_i}{\sum_{i=1}^n b_{\text{ext},i}} \quad (1)$$

where $b_{\text{ext},i}$ is the aerosol extinction coefficient (km^{-1}) at level i and Z_i is the altitude (km) at level i . In both CAM5 and CALIPSO, the lowest values of Z_α occur during boreal winter, while the highest values occur during boreal summer. However, CAM5 systematically underestimates Z_α , particularly during boreal summer in both

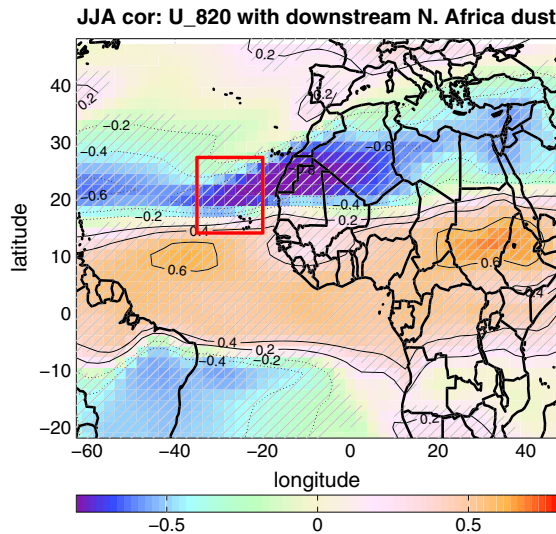


Figure 11. Pearson correlation of boreal summer CAM5 820 hPa zonal wind and area-averaged downstream North African dust burden. Gray hatches indicate regions where there is 95% confidence that the true correlation is not equal to zero, using a two-sample t test.

strong meridional gradient in the correlation pattern, with an inflection point near Cape Verde. This is evidence of a strong meridional gradient in the mean zonal wind at 820 hPa (not shown).

4.4. Evaluation of CESM North Atlantic Lower Tropospheric Cloud Fraction

Figure 12 shows 150 year seasonal averages of vertically integrated lower tropospheric cloud fraction over North Africa and the tropical-subtropical North Atlantic. Lower tropospheric cloud fraction is defined as the

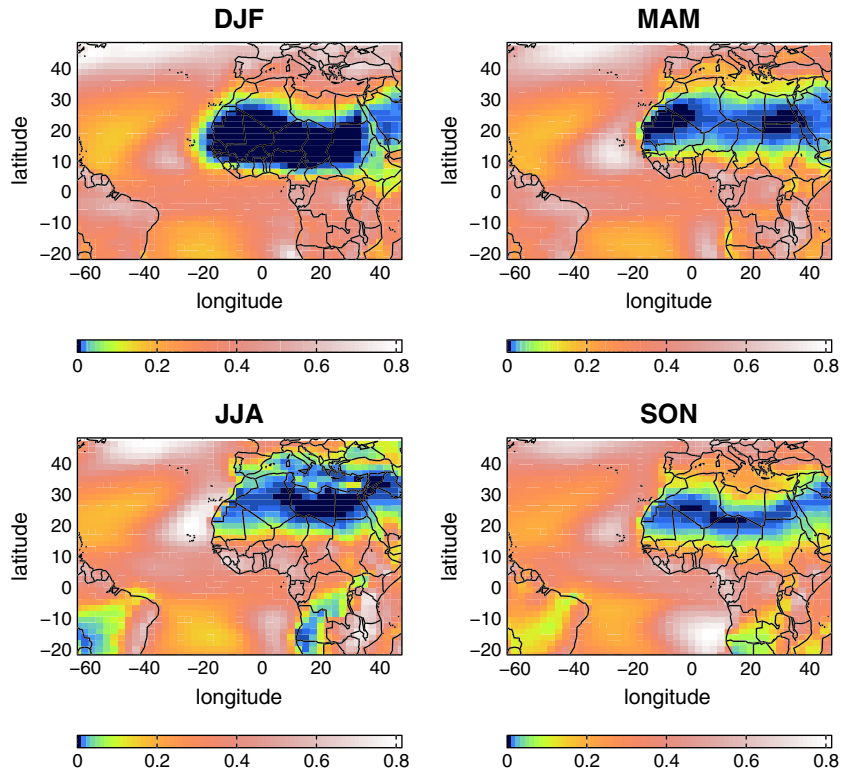


Figure 12. One hundred fifty year seasonal averages of CAM5 vertically integrated lower tropospheric cloud fraction.

regions. It is important to note that CALIPSO data used here to calculate mean extinction height are only available for 3 years, while the CAM5 simulation is 150 years.

4.3. Relationship of Lower Tropospheric Zonal Wind to Downstream North African Dust

Figure 11 shows a Pearson correlation of boreal summer 820 hPa zonal wind and downstream North African dust burden. Dust values were area averaged over the subtropical North Atlantic (10° N to 25° N; -35° W to -20° W) and correlated with 820 hPa zonal wind at each grid cell across the region shown. Hatched regions indicate areas where the true correlation is not equal to zero at the 95% confidence level, computed using a two-sample t test. Large negative correlation values (~ -0.8) over northwest Africa and the eastern subtropical North Atlantic indicate that increased mass of atmospheric dust downstream of North Africa is associated with stronger lower tropospheric easterly flow. In addition, there is a

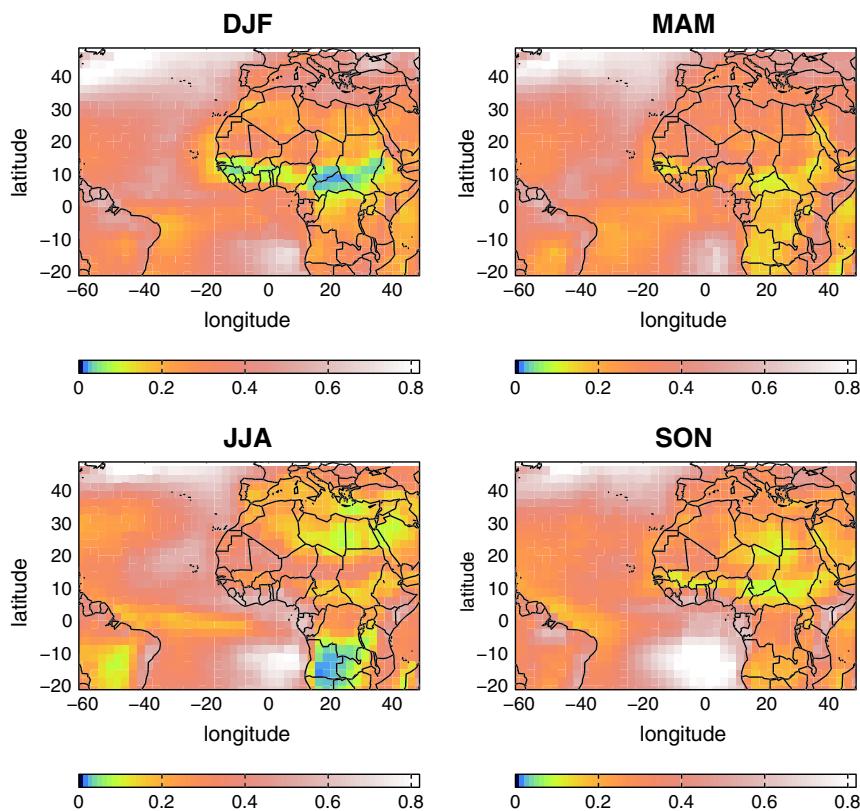


Figure 13. Seasonal averages of ISCCP low cloud fraction, from January 1984 to 2009.

seasonal average of percentage of cloud cover over a given grid cell, averaged over the 1000 hPa to 700 hPa layer. Subtropical North Atlantic cloud fraction downstream of high Saharan source regions of dust increases by up to 80% from boreal winter to boreal spring and summer. In addition, the location of maximum lower tropospheric cloud fraction shifts northward during the summer, coincident with the northward shift in downstream dust transport during that season. Middle-to-upper (i.e., above 700 hPa) tropospheric cloud fraction does not increase during the spring and summer over this region (not shown).

Figure 13 shows seasonal averages of ISCCP low-level cloud fraction, spanning from January 1984 to December 2009. Low-level cloud fraction is estimated using a random overlap correction, such that

$$\text{LLCF} = \text{LOW}/(1 - \text{HIGH} - \text{MID})$$

where LOW = ISCCP low-level cloud fraction, HIGH = ISCCP high-level cloud fraction, and MID = ISCCP midlevel cloud fraction. The random overlap correction is applied because ISCCP often misplaces low clouds into the midlevel category over strong inversions [Garay *et al.*, 2008] and if there are overlying cirrus [Mace *et al.*, 2006], and because ISCCP can only see low clouds unobscured by higher clouds [Rozendaal *et al.*, 1995]. Observed low-level cloud fraction downstream of high dust source regions increases substantially during boreal summer, but the increase is not as large as is seen in CESM. Like CESM, the highest values of ISCCP low-level cloud fraction shift northward downstream of North Africa during boreal summer. Large differences ISCCP and CESM can be found over the Sahara desert. ISCCP values are much higher in this region because ISCCP cannot distinguish between aerosol and cloud in regions where AOD is high, and because ISCCP may mistake the bright desert surface for cloud droplets [e.g., Engelstaedter *et al.*, 2006].

5. Relating North African Dust Transport to Subtropical Atlantic Lower Tropospheric Cloud Fraction Increase During Boreal Summer

The results from section 4 suggest a possible link between boreal summer North African dust transport and increased subtropical Atlantic lower tropospheric cloud fraction in CESM 1.0. Mahowald and Kiehl [2003] were

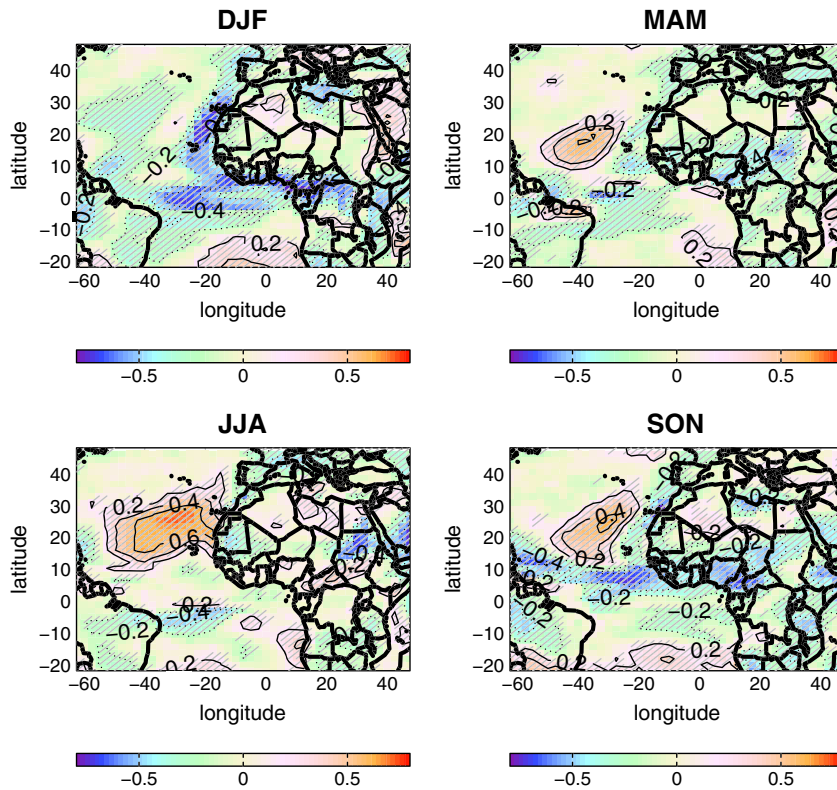


Figure 14. Pearson correlations of seasonally averaged CAM5 dust burden and lower tropospheric cloud fraction anomalies over North Africa and the tropical-subtropical North Atlantic. Gray hatches indicate regions where there is 95% confidence that the true correlation is not equal to zero, using a two-sample *t* test.

the first to correlate subtropical and tropical North Atlantic cloud cover with North African dust, using a 16 year subset of the ISCCP data set. They found that surface dust concentrations at the Barbados in situ observing site in the western subtropical Atlantic [Prospero and Nees, 1986] were moderately correlated with only low thin clouds over the subtropical North Atlantic, downstream of the Sahara desert source region. However, due to observational data constraints, the authors could not distinguish between a microphysical (Saharan dust acting as CCN for low thin clouds) or dynamical link between the two variables. Here we explore this relationship in CESM 1.0.

5.1. Dust Burden and Lower Tropospheric Cloud Fraction Correlation

Figure 14 shows Pearson correlations of seasonally averaged dust burden and lower tropospheric cloud fraction over North Africa and the tropical-subtropical North Atlantic. Hatched regions indicate areas where the true correlation is not equal to zero at the 95% confidence level, computed using a two-sample *t* test. During boreal spring, and particularly during boreal summer, a modest-to-strong correlation pattern emerges over the eastern subtropical North Atlantic, downstream of North Africa. This area is coincident with increases in both transported Saharan dust over the open ocean and increased lower tropospheric cloud fraction during these seasons. In contrast to positive correlations observed at lower levels, the correlation of middle and upper tropospheric cloud fraction to dust burden during these seasons is close to zero (not shown).

Figure 16 shows a scatterplot of boreal summer average dust burden anomalies (abscissa) and lower tropospheric cloud fraction anomalies (ordinate), area averaged over the modest-to-strong correlation region shown in Figure 14; each point represents a seasonal average anomaly value. Clearly, a strong linear relationship between the two variables exists over this region during boreal summer ($R \sim 0.75$). The seasonal anomalies of lower tropospheric cloud fraction over the subtropical North Atlantic during boreal summer are approximately 10–20% of the raw values over the 150 year simulation, while the seasonal anomalies of dust burden in this region are a similar fraction of raw values, but with several highly anomalous seasons where

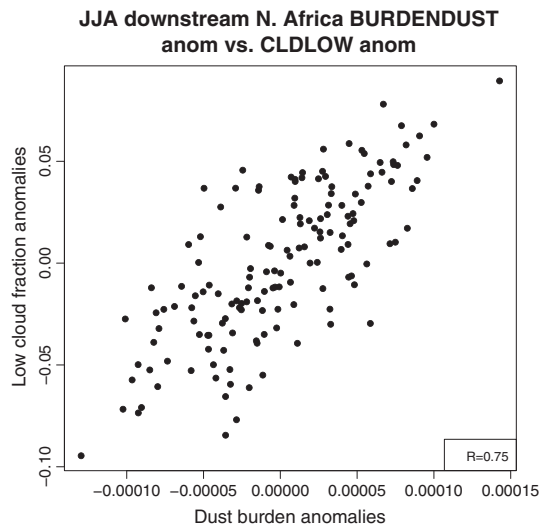


Figure 15. Scatterplot of boreal summer CAM5 average dust burden anomalies (abscissa; kg/m²) and lower tropospheric cloud fraction anomalies (ordinate; unitless), area averaged over the modest-to-strong correlation region shown in Figure 14.

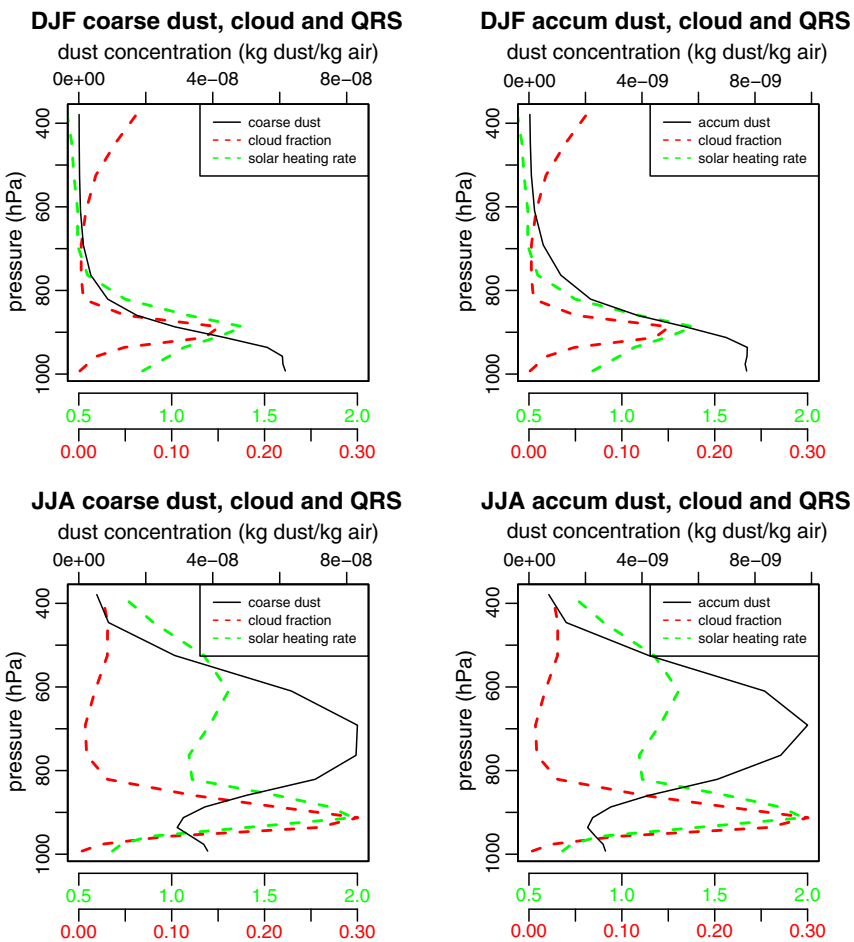


Figure 16. Vertical profiles of 150 year boreal winter (DJF) and summer (JJA) averages of CAM5 downstream North African coarse and accumulation mode dust concentration (black), cloud fraction (red), and solar heating rate (green).

the fraction increases to near 60% (not shown). Subsequent analyses are aimed at determining whether a microphysical or dynamical mechanism is primarily involved in linking the cloud variation to the fluctuating dust concentration over the eastern North Atlantic.

5.2. Vertical Structure of Downstream North African Dust, Cloud Fraction, and Solar Heating Rate

Figure 16 builds upon the results of Figures 14 and 15 to gain more insight into the strong boreal summer correlation between dust burden and lower tropospheric cloud fraction over the subtropical Atlantic. It plots vertical profiles of 150 year averages of coarse and accumulation mode dust concentration (black), cloud fraction (red), and solar heating rate (green) area averaged over the subtropical North Atlantic region downstream of North Africa during boreal winter (Figure 16, top row) and summer (Figure 16,

bottom row). During boreal winter, the maximum dust concentration is close to the surface, and cloud fraction is generally low over the subtropical North Atlantic region. However, a very different vertical structure is present during the summer, when the maximum dust concentration is located several hundred hectopascals above the maximum cloud fraction, which is located in the boundary layer (see also Figures 7 and 8). Additionally, the vertical structure of cloud fraction is very similar in both seasons, but the ~900 hPa maximum is nearly twice as large in the summer. This suggests that dust may be affecting clouds radiatively or dynamically in this region, but not microphysically, since the vertical structure of cloud fraction is distinct from that of dust concentration, but the magnitude of maximum boundary layer cloud fraction doubles when dust transport in the layer above increases.

In both boreal winter and summer, solar heating rate is at maximum near the top of the maximum cloud layer. This is due to weak solar absorption by cloud droplets and water vapor at the cloud top [Wood, 2012]. However, in boreal summer, a secondary maximum of solar heating rate emerges within the layer of maximum dust concentration. This additional heating due to solar absorption by dust will heat the air locally and decrease the amount of solar radiation reaching the lower troposphere. Both heating near the cloud top and cooling at the surface will promote lower tropospheric cloud growth by increasing inversion strength (i.e., dT/dz becomes more positive). Vertical profiles of air temperature during boreal summer over this region show a maximum near the bottom of the maximum dust layer around 750 hPa, but not near the maximum cloud layer around 900 hPa. This 750 hPa temperature maximum is absent during boreal winter, when dust concentrations are lower aloft than in the summer. This is further evidence supporting the hypothesis that dust is strengthening the boreal summer subtropical North Atlantic temperature inversion, at least in part by increased temperatures aloft due to solar absorption by advected North African dust. However, we must note that the likely overestimate of absorption from using the OPAC dust refractive indices means this inversion strengthening mechanism is likely overestimated by CESM [Albani *et al.*, 2014].

The high summertime correlation between dust burden and lower tropospheric cloud fraction in Figure 16 may be explained in several possible ways: (A) the correlation is spurious and has no physical significance; (B) dust particles advected off the North African continent are acting as cloud condensation nuclei in the lower troposphere [Rosenfeld *et al.*, 2001]; (C) dust particles advected off the North African continent reflect shortwave radiation back to space, heat the air locally due to solar absorption by the dust, cool the boundary layer, and promote lower tropospheric cloud growth by strengthening the lower tropospheric inversion and bringing the air closer to saturation [Koch and Del Genio, 2010]; (D) the correlation is driven by the response of both dust and cloud to another factor, such as vertical velocity. Although vertical velocity is related to inversion strength because of its influence on air temperature due to adiabatic heating and cooling, it can also be dynamically important in transporting quantities of dust away from or closer to the boundary layer. Hypothesis A appears unlikely, given the strong statistical significance of the results from the long CESM simulation and also the well-known radiative, dynamical, and microphysical impact of dust particles in the atmosphere. These impacts have been elucidated by a body of (aforementioned) previous studies that have explored hypotheses B and C in a variety of experimental situations. Hypothesis B can be eliminated because the maximum dust concentration (around 700 hPa) is located above the maximum cloud fraction (around 900 hPa). In addition, as mentioned previously, dust particles are usually associated with cold cloud ice nucleation rather than warm cloud droplet nucleation which must be at work in the low cloud structure under consideration here. However, coarse mode dust particles in CAM5 are large enough that droplets can form on them, in spite of relatively low hygroscopicity (0.068). In addition, the results from Figure 16 suggest that elevated summertime dust concentrations over the subtropical North Atlantic could potentially promote cloud growth due to their location above the boundary layer and above the maximum cloud layer. Results presented in the following sections further suggest that hypothesis C is a likely explanation for the link between boreal summer North African dust transport and lower tropospheric cloud growth in CESM 1.0. Hypothesis D will also be explored by looking at correlations of dust and cloud with a measure of vertical velocity.

5.3. EIS Calculation

To further test hypothesis C, we use model output to calculate Estimated Inversion Strength (EIS) over the subtropical North Atlantic region for boreal winter (when downstream North African dust concentration is low, and when the relationship between North African dust and lower tropospheric cloud fraction is weak)

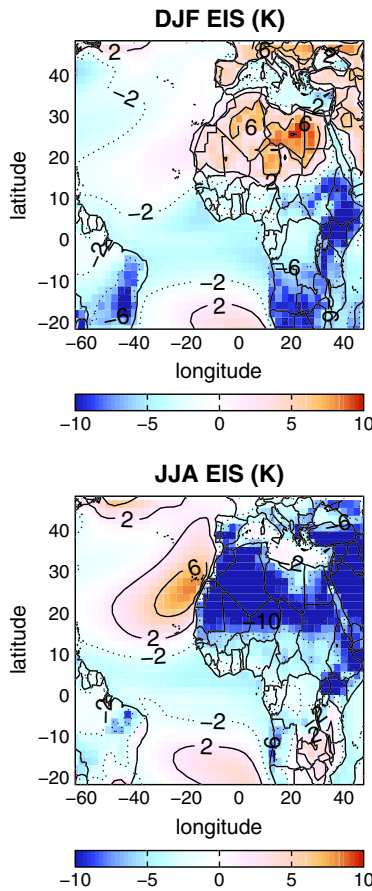


Figure 17. One hundred fifty year boreal winter and summer averages of CAM5 estimated inversion strength (K).

5.5. Composites of EIS on Most Dusty and Least Dusty Summers Downstream of North Africa

Figures 15–17 suggest that dust may be acting to increase EIS downstream of North Africa by cooling the boundary layer and/or heating the atmosphere near 700 hPa. However, it is still possible that the relationship between dust burden and lower tropospheric cloud fraction is coincidentally caused by the same underlying dynamics in the atmosphere. In addition, increased EIS during boreal summer could be a result of increased lower tropospheric cloud fraction alone, independent of North African dust. Figure 18 further investigates

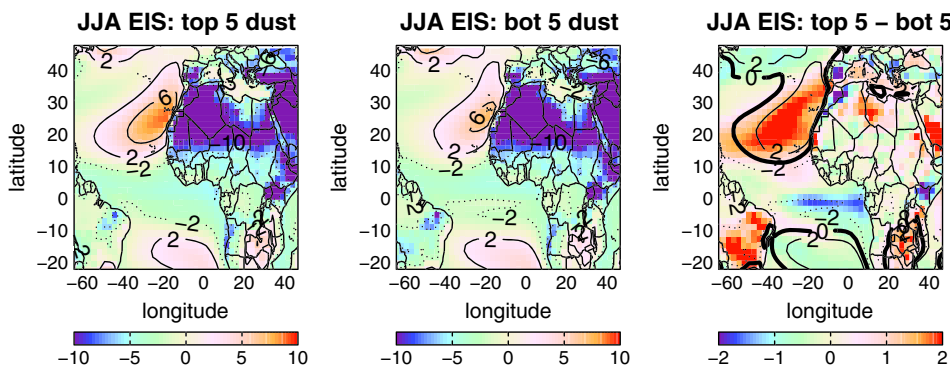


Figure 18. One hundred fifty year boreal summer averages of CAM5 estimated inversion strength (K) on the (left) five most dusty downstream North African seasons, (middle) five least dusty seasons, and the (right) difference between the top and bottom five seasons.

and boreal summer (when downstream North African dust concentration is high, and when the relationship between North African dust and lower tropospheric cloud fraction is strong). EIS is a formulation introduced by *Wood and Bretherton* [2006] that estimates boundary layer inversion strength, which promotes stratiform low cloud cover along western continental boundaries around the globe [*Myers and Norris*, 2013]. Recall that an inversion is defined as a layer in the atmosphere where $\frac{dT}{dz} > 0$. *Wood and Bretherton* [2006] note that EIS is a superior metric to Lower Tropospheric Stability, since it is independent from a region's background climatology. The calculation of EIS is summarized below and derived in *Wood and Bretherton* [2006].

EIS is defined as follows:

$$\text{EIS} = \text{LTS} - \Gamma_m^{850} \times (Z_{700} - Z_{\text{LCL}}) \quad (2)$$

where $\text{TS} = \theta_{700} - \theta_{\text{sfc}}$, Γ_m^{850} = moist adiabatic lapse rate centered at 850 hPa = $\Gamma_m(T_{\text{avg}}, 850 \text{ hPa})$; $T_{\text{avg}} = (T_{\text{sfc}} + T_{700})/2$, and $Z_{\text{LCL}} = \frac{R_d}{2 \times g_0} \times \ln\left(\frac{\text{SLP}}{P_{\text{LCL}}}\right)$. Therefore, $\text{EIS} = \text{EIS}(T_{\text{sfc}}, T_{\text{dew}}, T_{700}, Z_{700}, \text{SLP})$, where T_{dew} is the dew point temperature. All variables but T_{dew} can be acquired from CAM5 output; T_{dew} can be calculated using the Clausius-Clapeyron equation.

5.4. EIS Over the Subtropical North Atlantic During Boreal Summer

Figure 17 shows 150 year boreal winter and summer averages of estimated inversion strength (°K). Larger values of EIS indicate a stronger inversion near the boundary layer. Indeed, the largest values of EIS are found downstream of North Africa during boreal summer and are colocated with regions of maximum dust transport near 700 hPa and maximum cloud fraction near 900 hPa.

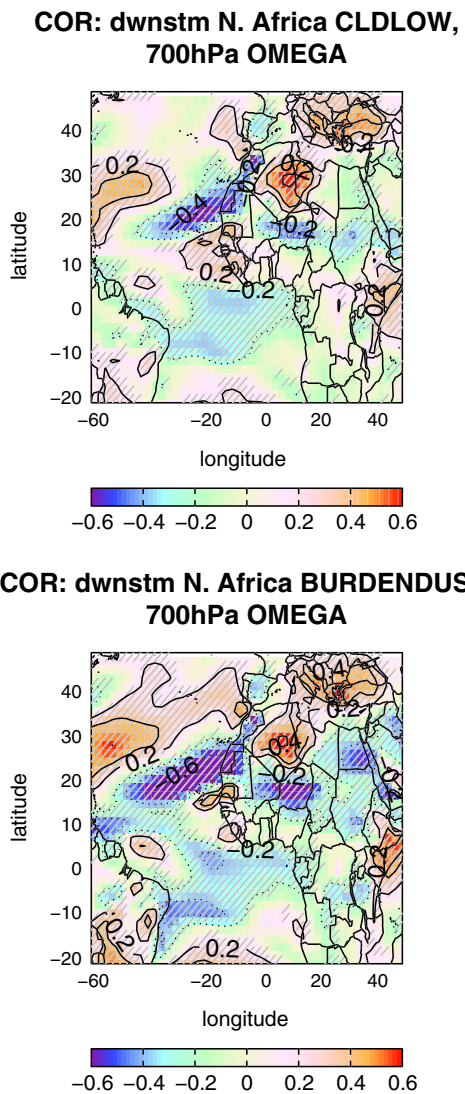


Figure 19. Pearson correlations of (top) average boreal summer CAM5 downstream North African lower tropospheric cloud fraction and 700 hPa omega anomalies and (bottom) downstream North African dust burden and 700 hPa omega anomalies. Gray hatches indicate regions where there is 95% confidence that the true correlation is not equal to zero, using a two-sample *t* test.

the descending branch of the Hadley Cell circulation. Myers and Norris [2013] showed observational evidence suggesting that enhanced subsidence reduces subtropical marine boundary layer cloudiness, which is consistent with the sign of the correlation in Figure 19 (top). In Figure 19 (bottom), values in this region are strongly negative, indicating that increased values of downstream North African dust burden anomalies are associated with decreased values of 700 hPa ω anomalies, which also means weakened subsidence. Figures 7 and 8 showed that in this region, boreal summer dust concentration is maximum around 700 hPa.

While we have shown evidence that dust increases inversion strength and therefore enhances lower tropospheric cloud fraction (hypothesis C), it is difficult to evaluate hypothesis D without a complementary CAM5 simulation that does not include the interactive dynamical and radiative effects of dust in the atmosphere. In addition, calculation of heat and moisture budgets using monthly data is insufficient to demonstrate that the presence of dust is weakening subsidence and therefore promoting lower tropospheric cloud growth. This hypothesis will be explored in future studies using daily or subdaily data, with a

this relationship by showing composites of EIS, averaged on the five most dusty (left) and five least dusty (middle) boreal summers over the downstream North African region. Figure 18 (right) shows the difference between Figure 18 (left) and Figure 18 (middle) and indicates that EIS increases by up to 20% in some regions on extremely dusty summers downstream of North Africa. This result suggests that the dust-low cloud relationship in this region is driven primarily by a semidirect dynamical effect rather than cloud microphysics, since both solar absorption and reflection by dust near 700 hPa promote increased inversion strength. But again, it is likely the semidirect effect is overestimated by CESM.

5.6. Relationship of Downstream North African Dust Burden and Lower Tropospheric Cloud Fraction to Vertical Velocity

Hypothesis D states that the correlation shown in Figure 14 is driven by the response of both dust and cloud to an external meteorological factor, such as vertical velocity. Figure 19 explores these relationships by showing Pearson correlations of boreal summer downstream North African dust burden anomalies with 700 hPa $\omega = dp/dt$ anomalies (top) and boreal summer downstream North African lower tropospheric cloud fraction anomalies with 700 hPa ω anomalies (bottom). Hatched regions indicate areas where the true correlation is not equal to zero at the 95% confidence level, computed using a two-sample *t* test. As shown in Figure 14, the area from around 20°N to 30°N, -40°W to -20°W is where boreal summer dust and low cloud anomalies were most strongly correlated.

In Figure 19 (top), values in this region are weakly to moderately negative, indicating that increased values of downstream North African low cloud anomalies are associated with decreased values of 700 hPa ω anomalies, which means weaker subsidence. Note that the mean 700 hPa ω field in this region is strongly positive due to large-scale subsidence associated with

the descending branch of the Hadley Cell circulation. Myers and Norris [2013] showed observational evidence suggesting that enhanced subsidence reduces subtropical marine boundary layer cloudiness, which is consistent with the sign of the correlation in Figure 19 (top). In Figure 19 (bottom), values in this region are strongly negative, indicating that increased values of downstream North African dust burden anomalies are associated with decreased values of 700 hPa ω anomalies, which also means weakened subsidence. Figures 7 and 8 showed that in this region, boreal summer dust concentration is maximum around 700 hPa.

comparison to a prescribed aerosol CAM5 simulation to further examine the relationship between weakened subsidence, increased dust burden, and increased cloud fraction anomalies.

6. Summary

In this study, we used a 150 year preindustrial CESM 1.0 simulation to investigate the seasonal cycle of dust burden and transport, circulation, and lower tropospheric cloud fraction over North Africa and the subtropical North Atlantic and employed simple statistical techniques and dynamical calculations to explain the semidirect mechanism relating boreal summer lower tropospheric transport of dust downstream of North Africa and lower tropospheric cloud cover over the eastern subtropical North Atlantic.

The model's seasonal cycle of aerosol optical depth near Cape Verde is strong and is consistent with AERONET observations in this region. The surface concentration of dust downstream of North Africa at Barbados is also in reasonable agreement with observations. Aerosol volume size distribution in CAM5 at Cape Verde peaks at a radius of approximately 2–3 μm , which is consistent with AERONET observations, though the magnitude is too small. Transport of dust downstream of North Africa is strongest during boreal summer, in association with the formation of the downward flank of the African easterly jet forms and persists into the fall. Vertical profiles of dust concentration and cloud fraction over the subtropical North Atlantic show that in the summer, the maximum dust concentration is near 700 hPa, while the maximum cloud fraction is near 900 hPa. Koch and Del Genio [2010] note that this is a favorable vertical setup for absorbing aerosols to stabilize the atmosphere below and enhance lower tropospheric stratiform clouds. In addition, during boreal spring and especially during boreal summer, lower tropospheric cloud fraction and dust burden are moderately to strongly correlated downstream of North Africa.

Solar heating rate increases during boreal summer near the location of maximum dust around 700 hPa, which increases inversion strength and promotes lower tropospheric cloud growth. Modeled EIS values increase by up to 60% during boreal summer over this region, indicating that lower tropospheric cloud growth there is caused by increased inversion strength in the boundary layer that appear to be related to increased dust transport off the North African coast. We also show that EIS increases by up to 20% during summers where dust burden downstream of North Africa is very high.

7. Discussion

Our results provide insight into effects of transported dust on warm phase low cloud growth and help further elucidate the complex relationships between dust emission, regional meteorology, and aerosol-cloud interactions over the subtropical North Atlantic, downstream of continental high source regions. Transported North African dust and lower tropospheric North Atlantic cloud variations from the 150 year CESM simulation are obtained using a model with a realistic seasonal cycle of dust and African easterly jet formation and improved parameterization of cloud microphysics [Gettelman et al., 2008; Gent et al., 2011; Neale et al., 2013]. The analyses from the simulation strongly suggest that African dust and low cloud cover over the eastern North Atlantic are dynamically linked and that transported African dust is enhancing lower tropospheric cloud cover over the open ocean via a semidirect mechanism [Koch and Del Genio, 2010] that is likely overestimated due to the assumed dust refractive index, which accentuates the sensitivity of such a modeling study to the absorptive properties of dust in the model used. The summertime transport of dust in the lower troposphere over the open ocean in CESM is consistent with observational studies that have investigated the mechanisms controlling the vertical structure of dust near the Saharan Planetary Boundary Layer [Cuesta et al., 2009; Knippertz and Todd, 2012]. Specifically, Figure 8 shows that during summer, there is a large relative increase in dust concentration above the boundary layer downstream of high source regions associated with the transport of dust by the lower tropospheric easterlies in the Saharan Air Layer. Our results also provide valuable insight on the long-term behavior of North African dust transport and its impact on lower tropospheric cloud growth, which is important due to the multiyear variability of North African boreal summer dust transport in CESM (not shown). In spite of the strong evidence for a semidirect mechanism presented in this work, other factors are likely to contribute to the increase in EIS over the subtropical North Atlantic during boreal summer, including warm air advection of the Saharan Air Layer in the midtroposphere and ocean upwelling associated with the Canary Current and should be explored further in future studies.

In complement to additional field measurements, further investigation of these relationships could prove useful using different global climate model simulations with realistic atmospheric models to represent the behavior of dust and low clouds in this region. One caveat in using global climate models to investigate aerosol-cloud interactions is that each model parameterizes both clouds and mineral dust emission and optical properties differently and often does so at coarse vertical resolution. It is for this reason that we encourage examination of these interactions using a variety of climate models with different representations of stratiform clouds and different dust emission models. A particularly useful extension of our work is to analyze daily variables in order to diagnose the dust-cloud interactions over the spring and summer in this region, which will be explored in future studies.

Acknowledgments

This study forms a portion of the Ph.D. dissertation of M.J.D. Funding was provided by NSF (AGS-1048995) and by the U.S. Department of Energy, Office of Science, Decadal and Regional Climate Prediction using Earth System Models (EaSM program). The Pacific Northwest National Laboratory is operated for the DOE by Battelle Memorial Institute under contract DE-AC06-76RLO 1830. We are grateful for the contribution made by Joseph M. Prospero (RSMAS, U. Miami), who provided us with the Barbados dust record. Many detailed and insightful comments and suggestions made by the anonymous reviewers have led to significant improvements in this paper. Thanks to Joel Norris and Timothy Myers (SIO) for clarifications and ideas regarding lower tropospheric warm phase clouds, Amato Evan (SIO) for literature references and useful discussions regarding seasonal variability of Saharan dust, Li Xu (SIO) and Dave Erickson (ORNL) for assistance in calculating aerosol size distribution, and Didier Tanre and Joseph M. Prospero for their efforts in establishing and maintaining the Cape Verde and Barbados AERONET sites, respectively, used in this investigation. The CAM5 data used in this study can be accessed via an email inquiry (mdeflori@ucsd.edu).

References

- Ackerman, S., and H. Chung (1992), Radiative effects of airborne dust on regional energy budgets at the top of the atmosphere, *J. Appl. Meteorol.*, **31**, 223–233.
- Albani, S., N. M. Mahowald, A. T. Perry, R. A. Scanza, C. S. Zender, N. G. Heavens, V. Maggi, J. F. Kok, and B. L. Otto-Biesner (2014), Improved dust representation in the Community Atmosphere Model, *J. Adv. Model. Earth Syst.*, doi:10.1002/2013MS000279.
- Albrecht, B. A. (1989), Aerosols, cloud microphysics and fractional cloudiness, *Science*, **245**, 1227–1230.
- Ashpole, I., and R. Washington (2013), A new high-resolution central and western Saharan summertime dust source map from automated satellite dust plume tracking, *J. Geophys. Res. Atmos.*, **118**, 6981–6995, doi:10.1002/jgrd.50554.
- Ault, A. P., C. R. Williams, A. B. White, P. J. Neiman, J. M. Cramean, C. J. Gaston, F. M. Ralph, and K. A. Prather (2011), Detection of Asian dust in California orographic precipitation, *J. Geophys. Res.*, **116**, D16205, doi:10.1029/2010JD015351.
- Bretherton, C. S., and S. Park (2009), A new moist turbulence parameterization in the community atmosphere model, *J. Clim.*, **22**, 3422–3448, doi:10.1175/2008JCLI2556.1.
- Carslaw, K. S., O. Boucher, D. V. Spracklen, G. W. Mann, J. G. L. Rae, S. Woodward, and M. Kulmala (2010), A review of natural aerosol interactions and feedbacks within the Earth system, *Atmos. Chem. Phys.*, **10**(4), 1701–1737.
- Chiapello, I., C. Moulin, and J. M. Prospero (2005), Understanding the long-term variability of African dust transport across the Atlantic as recorded in both Barbados surface concentrations and large-scale Total Ozone Mapping Spectrometer (TOMS) optical thickness, *J. Geophys. Res.*, **110**, D18S10, doi:10.1029/2004JD005132.
- Cuesta, J., J. H. Marsham, D. J. Parker, and C. Flamant (2009), Dynamical mechanisms controlling the vertical redistribution of dust and the thermodynamic structure of the west Saharan atmospheric boundary layer during summer, *Atmos. Sci. Lett.*, **10**, 34–42, doi:10.1002/asl.207.
- Darwin, C. (1897), *Journal of Researches into the Natural History and Geology of the Countries Visited During the Voyage of the H.M.S. Beagle Round the World, Under the Command of Capt. Fitz Roy, R.N.* 2nd ed., 519 pp., D. Appleton and Company, New York.
- DeMott, P. J., D. J. Cziczo, A. J. Prenni, D. M. Murphy, S. M. Kreidenweis, D. S. Thomson, R. Borys, and D. C. Rogers (2003), Measurements of the concentration and composition of nuclei for cirrus formation, *Proc. Natl. Acad. Sci. U.S.A.*, **100**, 14,655–14,660.
- Dubovik, O., and M. D. King (2000), A flexible inversion algorithm for retrieval of aerosol optical properties from Sun and sky radiance measurements, *J. Geophys. Res.*, **105**, 20,673–20,696, doi:10.1029/2000JD900282.
- Engelstaedter, S., I. Tegen, and R. Washington (2006), North African dust emissions and transport, *Earth Sci. Rev.*, **79**(1–2), 73–100, doi:10.1016/j.earscirev.2006.06.004.
- Evan, A. T., and S. Mukhopadhyay (2010), African dust over the northern tropical Atlantic: 1955–2008, *J. Appl. Meteorol. Climatol.*, **49**(11), 2213–2229, doi:10.1175/2010AMC2485.1.
- Evan, A. T., A. K. Heidinger, and M. J. Pavolonis (2006), Development of a new over-water Advanced Very High Resolution Radiometer dust detection algorithm, *Int. J. Remote Sens.*, **27**(18), 3903–3924, doi:10.1080/01431160600646359.
- Evan, A. T., D. J. Vimont, A. K. Heidinger, J. P. Kossin, and R. Bennartz (2009), The role of aerosols in the evolution of tropical North Atlantic Ocean temperature anomalies, *Science*, **324**(5928), 778–781, doi:10.1126/science.1167404.
- Garay, M. J., S. P. de Szeke, and C. M. Moroney (2008), Comparison of marine stratocumulus cloud top heights in the southeastern Pacific retrieved from satellites with coincident ship-based observations, *J. Geophys. Res.*, **113**, D18204, doi:10.1029/2008JD009975.
- Gent, P. R., et al. (2011), The Community Climate System Model version 4, *J. Clim.*, **24**, 4973–4991, doi:10.1175/2011JCLI4083.1.
- Gettelman, A., H. Morrison, and S. J. Ghan (2008), A new two-moment bulk stratiform cloud microphysics scheme in the NCAR Community Atmosphere Model (CAM3), Part II: Single-column and global results, *J. Clim.*, **21**, 3660–3679, doi:10.1175/2008JCLI2116.1.
- Ghan, S. J., and R. A. Zaveri (2007), Parameterization of optical properties for hydrated internally mixed aerosol, *J. Geophys. Res.*, **112**, D10201, doi:10.1029/2006JD007927.
- Ginoux, P., J. M. Prospero, T. E. Gill, N. C. Hsu, and M. Zhao (2012), Global-scale attribution of anthropogenic and natural dust sources and their emission rates based on MODIS Deep Blue aerosol products, *Rev. Geophys.*, **50**, RG3005, doi:10.1029/2012RG000388.
- Hess, M., P. Koepke, and I. Schult (1998), Optical properties of aerosols and clouds: The software package OPAC, *Bull. Am. Meteorol. Soc.*, **79**(5), 831–844.
- Huneeus, N., et al. (2011), Global dust model intercomparison in Aerocom Phase I, *Atmos. Chem. Phys.*, **11**, 7781–7816.
- Hurrell, J. W., et al. (2013), The Community Earth System Model: A framework for collaborative research, *Bull. Am. Meteorol. Soc.*, **94**, 1339–1360, doi:10.1175/BAMS-D-12-00121.
- Jones, A., D. L. Roberts, and A. Slingo (1994), A climate model study of indirect radiative forcing, *Nature*, **370**, 450–453.
- Kaufman, Y. J., I. Koren, L. A. Remer, D. Tanré, P. Ginoux, and S. Fan (2005), Dust transport and deposition observed from the Terra Moderate Resolution Imaging Spectroradiometer (MODIS) spacecraft over the Atlantic Ocean, *J. Geophys. Res.*, **110**, D10S12, doi:10.1029/2003JD004436.
- Kiehl, J. T., and B. P. Briegleb (1993), The relative roles of sulfate aerosols and greenhouse gases in climate forcing, *Science*, **260**, 311–314, doi:10.1126/science.260.5106.311.
- Klocke, D., R. Pincus, and J. Quasas (2011), On constraining estimates of climate sensitivity with present-day observations through model weighting, *J. Clim.*, **24**, 6092–6099.

- Knippertz, P., and M. C. Todd (2012), Mineral dust aerosols over the Sahara: Meteorological controls on emission and transport and implications for modeling, *Rev. Geophys.*, 50, RG1007, doi:10.1029/2011RG000362.
- Koch, D., and A. D. Del Genio (2010), Black carbon absorption effects on cloud cover: Review and synthesis, *Atmos. Chem. Phys.*, 10, 7685–7696, doi:10.5194/acp-10-7685-2010.
- Koffi, B., et al. (2012), Application of the CALIOP layer product to evaluate the vertical distribution of aerosols estimated by global models: AeroCom phase I results, *J. Geophys. Res.*, 117, D10201, doi:10.1029/2011JD016858.
- Kok, J. (2011), A scaling theory for the size distribution of emitted dust aerosols suggests climate models underestimate the size of the global dust cycle, *Proc. Natl. Acad. Sci. U.S.A.*, 108, 1016–1021, doi:10.1073/pnas.1014798108.
- Leaitch, W. R., G. A. Isaac, J. W. Strapp, C. M. Banic, and H. A. Wiebe (1992), The relationship between cloud droplet number concentrations and anthropogenic pollution: Observations and climatic implications, *J. Geophys. Res.*, 97(D2), 2463–2474, doi:10.1029/91JD02739.
- Liu, X., et al. (2012), Toward a minimal representation of aerosols in climate models: Description and evaluation in the Community Atmosphere Model CAM5, *Geosci. Model Dev.*, 5(3), 709–739, doi:10.5194/gmd-5-709-2012.
- Lohmann, U., and J. Feichter (2005), Global indirect aerosol effects: A review, *Atmos. Chem. Phys.*, 5, 715–737.
- Mace, G. G., et al. (2006), Cloud radiative forcing at the Atmospheric Radiation Measurement Program Climate Research Facility: 1. Technique, validation, and comparison to satellite-derived diagnostic quantities, *J. Geophys. Res.*, 111, D11S90, doi:10.1029/2005JD005921.
- Mahowald, N. M., and L. M. Kiehl (2003), Mineral aerosol and cloud interactions, *Geophys. Res. Lett.*, 30(9), 1475, doi:10.1029/2002GL016762.
- Mahowald, N. M., et al. (2010), Observed 20th century desert dust variability: Impact on climate and biogeochemistry, *Atmos. Chem. Phys.*, 10(22), 10,875–10,893, doi:10.5194/acp-10-10875-2010.
- Marticorena, B., B. Chatenet, J.-L. Rajot, S. Traoré, M. Coulibaly, A. Diallo, I. Koné, A. Maman, T. Ndiaye, and A. Zakou (2010), Temporal variability of mineral dust concentrations over West Africa: Analyses of a pluriannual monitoring from the AMMA Sahelian Dust Transect, *Atmos. Chem. Phys.*, 10, 8899–8915, doi:10.5194/acp-10-8899-2010.
- Martin, J. H. (1990), Glacial-interglacial CO₂ change: The iron hypothesis, *Paleoceanography*, 5(1), 1–13, doi:10.1029/PA005i001p00001.
- Moulin, C., C. E. Lambert, F. Dulac, and U. Dayan (1997), Control of atmospheric export of dust from North Africa by the North Atlantic Oscillation, *Nature*, 387, 691–694.
- Myers, T. A., and J. R. Norris (2013), Observational evidence that enhanced subsidence reduces subtropical marine boundary layer cloudiness, *J. Clim.*, 26, 7507–7524, doi:10.1175/JCLI-D-12-00736.1.
- Neale, R. B., J. Richter, S. Park, P. H. Lauritzen, S. J. Vavrus, P. J. Rasch, and M. Zhang (2013), The mean Climate of the Community Atmosphere Model (CAM4) in forced SST and fully coupled experiments, *J. Clim.*, 26, 5150–5168, doi:10.1175/JCLI-D-12-00236.1.
- Okin, G., N. Mahowald, O. Chadwick, and P. Artaxo (2004), The impact of desert dust on the biogeochemistry of phosphorus in terrestrial ecosystems, *Global Biogeochem. Cycles*, 18, GB2005, doi:10.1029/2003GB002145.
- Park, S., and C. S. Bretherton (2009), The University of Washington shallow convection and moist turbulence schemes and their impact on climate simulations with the Community Atmosphere Model, *J. Clim.*, 22, 3449–3469, doi:10.1175/2008JCLI2557.1.
- Penner, J. E., et al. (2001), Aerosols, their direct and indirect effects, in *Climate Change 2001: The Scientific Basis. Contribution of Working Group I to the Third Assessment Report of the Intergovernmental Panel on Climate Change*, edited by J. T. Houghton et al., pp. 289–348, Cambridge Univ. Press, Cambridge, U.K.
- Petters, M. D., and S. M. Kreidenweis (2007), A single parameter representation of hygroscopic growth and cloud condensation nucleus activity, *Atmos. Chem. Phys.*, 7(8), 1961–1971.
- Prospero, J. M., and E. Bonatti (1968), Continental dust in the atmosphere of the Eastern Equatorial Pacific, *J. Geophys. Res.*, 74(13), 3362–3371, doi:10.1029/JC074i013p03362.
- Prospero, J. M., and P. J. Lamb (2003), African droughts and dust transport to the Caribbean: Climate change implications, *Science*, 302(5647), 1024–1027.
- Prospero, J. M., and R. T. Nees (1986), Impact of the North African drought and El Niño on mineral dust in the Barbados trade wind, *Nature*, 320, 735–738, doi:10.1038/320735a0.
- Prospero, J. M., E. Bonatti, C. Schubert, and T. N. Carlson (1970), Dust in the Caribbean atmosphere traced to an African dust storm, *Earth Planet. Sci. Lett.*, 9, 287–293.
- Rosenfeld, D., Y. Rudich, and R. Lahav (2001), Desert dust suppressing precipitation: A possible desertification feedback loop, *Proc. Natl. Acad. Sci. U.S.A.*, 98, 5975–5980.
- Rosenfeld, D., W. L. Woodley, D. Axisa, E. Freud, J. G. Hudson, and A. Givati (2008), Aircraft measurements of the impacts of pollution aerosols on clouds and precipitation over the Sierra Nevada, *J. Geophys. Res.*, 113, D15203, doi:10.1029/2007JD009544.
- Rosoww, W., and R. Schiffer (1991), ISCCP cloud data products, *Bull. Am. Meteorol. Soc.*, 72, 2–20.
- Rozendaal, M. A., C. B. Leovy, and S. A. Klein (1995), An observational study of diurnal variations of marine stratiform cloud, *J. Clim.*, 8, 1795–1809.
- Sassen, K., P. J. DeMott, J. M. Prospero, and M. R. Poellot, (2003), Saharan dust storms and indirect aerosol effects on clouds: CRYSTAL-FACE results, *Geophys. Res. Lett.*, 30(12), 1633, doi:10.1029/2003GL017371.
- Seinfeld, J. H., and S. N. Pandis (2012), *Atmospheric Chemistry and Physics: From Air Pollution to Climate Change*, 2nd ed., John Wiley, Hoboken, N. J.
- Sinyuk, A., O. Torres, and O. Dubovik (2003), Combined use of satellite and surface observations to infer the imaginary part of refractive index of Saharan dust, *Geophys. Res. Lett.*, 30(2), 1081, doi:10.1029/2002GL016189.
- Smirnov, A., B. N. Holben, T. F. Eck, O. Dubovik, and I. Slutsker (2001), Cloud-screening and quality control algorithms for the AERONET database, *Remote Sens. Environ.*, 73(3), 337–349.
- Smoydzin, L., A. Teller, H. Tost, M. Fnais, and J. Lelieveld (2012), Impact of mineral dust on cloud formation in a Saharan outflow region, *Atmos. Chem. Phys.*, 12, 11,383–11,393, doi:10.5194/acp-12-11383-2012.
- Sokolik, I. N., D. M. Winker, G. Bergametti, D. A. Gillette, G. Carmichael, Y. J. Kaufman, L. Gomes, L. Schuetz, and J. E. Penner (2001), Introduction to special section: Outstanding problems in quantifying the radiative impacts of mineral dust, *J. Geophys. Res.*, 106(D16), 18,015–18,027, doi:10.1029/2000JD900498.
- Stevens, B., and G. Feingold (2009), Untangling aerosol effects on clouds and precipitation in a buffered system, *Nature*, 461(7264), 607–13, doi:10.1038/nature08281.
- Tegen, I. (2003), Modeling soil dust aerosol in the climate system: An overview, *Quart. Sci. Rev.*, 22, 1821–1834.
- Tegen, I., A. A. Lacis, and I. Fung (1996), The influence on climate forcing of mineral aerosols from disturbed soils, *Nature*, 380, 419–422, doi:10.1038/380419a0.
- Twomey, S. (1974), Pollution and the planetary albedo, *Atmos. Environ.*, 8, 1251–1256.

- Wood, R. (2012), Stratocumulus Clouds, *Mon. Weather Rev.*, 140, 2373–2423, doi:10.1175/MWR-D-11-00121.1.
- Wood, R., and C. S. Bretherton (2006), On the relationship between stratiform low cloud cover and lower-tropospheric stability, *J. Clim.*, 19, 6425–6432, doi:10.1175/JCLI3988.1.
- Yokohata, T., M. J. Webb, M. Collins, K. D. Williams, M. Yoshimori, J. C. Hargreaves, and J. D. Annan (2010), Structural similarities and differences in climate responses to CO₂ increase between two perturbed physics ensembles, *J. Clim.*, 23, 1392–1410.
- Zender, C., H. Bian, and D. Newman (2003), Mineral Dust Entrainment and Deposition (DEAD) model: Description and 1990s dust climatology, *J. Geophys. Res.*, 108(D14), 4416, doi:10.1029/2002JD002775.